Direct observation of the microfiltration of yeast cells at the micro-scale: Characterization of cake properties

Alberto Valencia, Claude Lemen, Christophe Ellero, Christine Lafforgue-Baldas, Jeffrey F. Morris, Philippe Schmitz

Direct observation of the microfiltration of yeast cells at the micro-scale: characterization of cake properties

Alberto Valencia[a]* · Claude LeMen[b] · Christophe Ellero[b] · Christine Lafforgue-Baldas[b] · · Jeffrey F. Morris[c] · Philippe Schmitz[b]

[a)] FERMAT, Université de Toulouse, INSA, TBI, Avenue de Rangueil, 135, F-31077 Toulouse, France

*Corresponding author:

E-mail address: schmitz@insa-toulouse.fr (P. Schmitz)

Tel : +33 5 61 55 97 70

[b)] Université de Toulouse, INSA, TBI, Avenue de Rangueil, 135, F-31077 Toulouse, France

[c)] Levich Institute and Dept. of Chemical Engineering, CUNY City College of New York, 140th Street and Convent Avenue, New York, NY 10031

Abstract

This study examines the accumulation of yeast cells at the membrane surface and the morphology of the formed cake through microscale monitoring and analysis of the microfiltration process. An original dead-end microfiltration device with a model membrane was designed and coupled with an optical imaging system to provide direct observation from the side, allowing in-situ real time study of the filtration operation (Valencia et al. 2020 [1]). Here, the deposition of yeast cells, monodispersed and polydispersed particles, in the same size range that yeast cells, was analyzed. Image processing was used to perform a quantitative characterization of cake morphological properties in terms of height, porosity, permeability, Kozeny coefficient and specific resistance. The cakes formed by monodispersed spherical and non-spherical rigid particles exhibit a similar incompressible behavior with higher porosity than yeast cakes, with mean porosity values of 0.38 for the rigid particles and 0.15 for the yeast at the end of the filtration run, respectively. The cake obtained by the microfiltration of a model suspension of polydispersed particles close to yeast size and shape is more compact (porosity of 0.29) and less permeable. However, polydispersity does not fully explain yeast cake properties, in particular its compressibility. Indeed, the yeast cake has a high compressibility index n = 1.1, which is reflected in a significant volume expansion of the yeast cake after transmembrane pressure was removed.

Keywords: Microfiltration; Yeast; Model particle; Compressible cake

Abbreviations:

C: particle concentration above the membrane

CGM: cake growth monitoring module

$\overline{h}o$: measured average cake height

K_C: cake permeability

K_K: Kozeny coefficient

m: deposited mass per membrane surface unit

n: compressibility index

NS: non-spherical, peanut shape particle suspension

PCM: particle concentration module

PVM: particle velocimetry module

R_C: cake hydraulic resistance

R_M: membrane hydraulic resistance

R_T: total hydraulic resistance

S: spherical particle suspension

SD: polydisperse particle suspension

Sp: specific surface

U: average velocity at which particle approach membrane

α_C: cake specific resistance

β: specific resistance coefficient

ΔP: pressure difference

ϵ: porosity

ρ: density

μ: dynamic viscosity

1 Introduction

Particle transport and separation processes take place in many industrial sectors. Among them, membrane filtration is widely used in biotechnology and the pharmaceutical industry [2], the drinking water and waste water treatment sectors [3], [4] and the food and beverage industry [5]. It is natural then to seek for new ways to optimize the filtration performance. Membrane fouling is one of the main features hindering the filtration performance through mechanisms including sieving, bridging and particle aggregation [6], which always results in the permeate flux decline and a lower efficiency of the process.

In order to overcome such filtration drawbacks, many approaches have been studied like surface modification [7], [8], different membrane configurations [9], [10], the optimization of filtration operational conditions [11], [12]. While there is important research on antifouling features of some membrane surfaces, there is also a significant body of work on different ways to recondition the membrane performance to its initial state through cleaning methods as backwash [13], [14]. Previous research contributes to attenuate fouling, however, clogging and cake formation are still present. It is therefore still relevant to better understand the transport properties related to these phenomena.

While fouling has been studied at a macroscopic level, it has been approached at a smaller scale (particles, cells and pore scale) less exhaustively. Numerous studies have provided guidance toward better understanding of the process and made it possible to optimize, yet there are still many unsettled issues, particularly with regards to separation of bioparticles such as microorganisms. Research aiming to predict filtration process decay resulted in different theoretical and empirical fouling models for model particles [15]–[17], proteins [18], [19], and microorganisms [20]–[22]. When sieving is the main fouling mechanism, the later performance of the process is mostly related to the cake build-up on the filter unit. This behavior is approached by the classical filtration theory for which the hydraulic resistance of the deposit is calculated using the Carman-Kozeny relation. This could be a pertinent approach for non-compressible cakes of monodispersed particles, but experimental results differ from the predicted values for cakes that exhibit a compressible behavior. Many parameters usually assumed as constants in the Carman-Kozeny formula vary as the cake undergoes compression. The porosity of the cake progressively decreases, with significant impact on the cake resistance; the tortuosity value describing the cake capillaries and the pore shape may also change. This behavior depends on the mechanical properties of the filtered matter forming the cake, thus influencing the cake resistance and the loss of efficiency of the filtration process.

A better understanding of the filtration mechanisms at the microscale, especially for microorganisms, is key to fulfill the lack of information regarding filtration cake structure, morphology and porosity distribution. It is towards a more accurate description of the cake formation mechanisms and the resulting cake properties that different *in-situ* and non-invasive techniques that probe at the foulants level (particles, microorganisms) have been developed. Non-invasive techniques are mainly classified as optical and non-optical [23]. Optical probes include light scattering principles and are usually coupled to image post-processing analysis. Laser based techniques like triangulometry [24] and refractometry [25], [26] were used to measure in real-time the cake layer height and concentration gradients respectively, with a resolution about 2 – 5 µm. This resolution remains coarse relative to the size of typical micro-pollutants. Le Clech et al. [27] compared three tools for the study of the fouling phenomenon. From the scanning electron microscopy (SEM and ESEM) and the confocal laser scanning microscopy (CLSM), only the direct observation (DO) allowed *in-situ*, real-time and non-invasive data acquisition; however, it offered the lowest resolution (~10 µm). According to several reviews comparing the applicability of different techniques for studying the fouling phenomenon [28], [29], DO reach an enhanced

resolution of ~1 µm [30], [31]. Particularly, the suitability of CLSM for performing *in-situ* and non-invasive data acquisition was highlighted as the data acquisition rate of this tool remains insufficient for a real-time analysis [32], [33].

Despite its acquisition rate CLSM have been proposed to observe solutes smaller than the resolution in optical microscopy using laser excitation and sample fluorescent labelling. Recent work introduced by the CLSM use fluorescence to obtain 3D information as a stack of multiple planes at different depths, or focal planes, of the studied sample. The work by Ben Hassan [34], [35] used the CLSM for direct observation to acquire 3D images of the filtration cake. The work elucidated the first stage of particle deposition on the membrane and the later arrangement of the first layers of particles. The difficulties related to this technique are associated with the laser excitation. Laser penetration is of limited depth (~ 40 µm for yeast cakes), which limits the thickness of the deposit that one can inspect. Despite its resolution in the lateral (x and y) directions (<1µm), in the vertical (z) the scanned samples can be distorted.

Usually direct observation techniques (DO) combine an optical microscope with a camera. The DO set-up is coupled to a specially machined microsystem device. In the study of transport and separation, DO was initially used to observe particle deposition on the membrane surface [36], [37]. The DO technique allows the direct observation of cake formation at the membrane surface by the side. It differs from classical DOTM technique which allows the direct observation through the membrane, i.e., in the direction perpendicular to the membrane surface. The main drawbacks remain the limited optical depth and the focal plane of the observation. Recent work by Laar et al. [16] used DO from the side to study clogging phenomenon in dead-end filtration. They studied the flow through different pore geometries and filter configurations using particle image velocimetry (PIV); then they related the flow to particle aggregation inside the pores, which is the main cause of pore constriction. Further work in crossflow microfiltration shed light on the pore communication, relating the probability of a pore being clogged once their neighbors have been already obstructed [38].

In the work described in this paper, the previously validated dead end microfiltration system [1] was used to study the accumulation of yeast cells on a model membrane. This microsystem was used to analyze the behavior of living cell suspensions near the membrane during the initial stage of cake formation and the transition to fully developed cakes. A series of experiment using direct observation by the side (DO) have been performed for the filtration of four different suspensions: a suspension of cultivated yeast (*Saccharomyces cerevisiae*) and three suspensions of model particles with different size and shape distributions. Monodispersed suspensions of spherical and non-spherical particles as well as polydispersed particles were used to model features of the yeast cell suspensions and to better understand the effect of the morphology and size distribution on cake properties. The dead-end operating condition was chosen as it is suitable for analyzing the first layers of cake and the first stage of cake formation. Even though crossflow operation condition is widely used in the industry to reduce fouling phenomena, particles still accumulate at the membrane surface in a fashion similar to the dead-end case as the flow direction in the vicinity of the membrane in the normal direction, i.e. perpendicular to the filtration surface [35]. In the present study, cake formation is studied in its initial forming stage, which corresponds the zone where the velocity profile is perpendicular to the membrane in crossflow filtration as it is for dead-end configuration [39]. In addition, the dead-end operating condition is particularly simple for performing the mass balance, which could be a source of inaccuracy in previous studies using crossflow operation mode [29].

2 Materials and methods

2.1 Experimental set-up and protocol

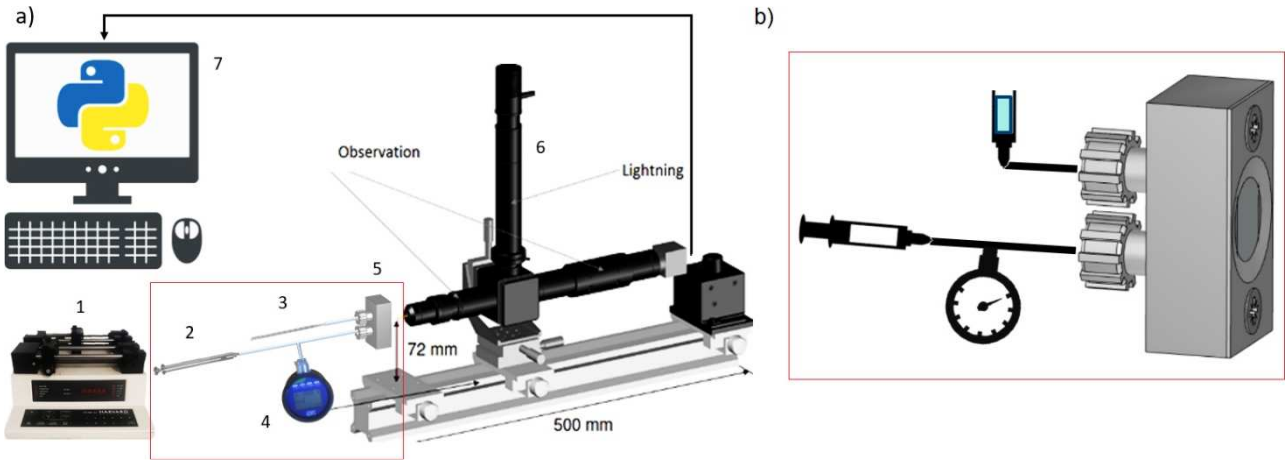

Figure 1. Scheme of the experimental set-up. 1) Syringe pump. 2) Syringe. 3) Reservoir. 4) Manometer. 5) Cell support. 6) Optical bench. 7) Acquisition computer. b) Scheme of the cell support and connectivity to the syringe pump, reservoir and manometer.

The original direct observation (DO) experimental set-up was previously developed for studying the dead-end filtration of model particles and is used here to analyze the cake growth for the filtration of yeast cell suspensions. The system is fully detailed in a previous paper [1]. The microfiltration unit is made in silicon, and it consists of a straight rectangular channel with a filter in the middle, the inlet and the outlet. Photolithography technique was used for the microfabrication of the filtration unit in partnership with Toulouse LAAS-CNRS laboratory. The filter membrane is composed of multiple parallel slots regularly arranged in different configurations. The filtration units are referred by the slot width *C* (2 and 4 µm), and the slot distance (3 and 16 µm) *Pe*, with this notation indicating periodicity. The cell geometry information is summarized in Table 1. The channel is 11.5 mm long, with a cross-section of 1 mm in width and 30 µm in depth.

Table 1. Microfiltration cell geometries

Membrane reference	Slot width, C (µm)	Periodicity, Pe (µm)	Slot distance d_p (µm)
C2Pe5	2	5	3
C4Pe20	4	20	16

A microscope objective attached to a camera (Basler acA 1920-155µm) is used for real-time imaging and data acquisition (Figure 1a). A syringe pump (Harvard Apparatus 33) provides a flowrate in the range of 1 to 20 µl/min. A manometer (Digital pressure gauge Type E2 - Sika) is used to measure the pressure in the system. Using the syringe pump the system is filled meticulously to avoid the presence of air bubbles, and then a constant flow of 10 µl/min is established; for the current experiments, the flow is characterized by Stokes regime (Reynold's number < 1). After the stationary flow condition is reached, the suspension is injected. Filtration starts and real-time imaging and data acquisition is launched when the first cells/particles appear in the observation domain. The experiments are conducted at a constant flowrate of 10µl/min and the pressure variations are recorded.

The estimate of the retention of suspended particles/cells must be accurate to perform a mass balance. The yeast suspension experiments were exclusively performed using the C2Pe5 filters units, which were the only ones with a pore size of 2 µm that guarantees the sieving of all the cells. This allows a better estimate of cell deposition. However, as these filtration units are more complex to manufacture, they are only used for the filtration of yeast. The previous paper [1] explored the effect of the different filter geometries on the cake structure for monodispersed spherical particles (8.4 µm diameter); it was shown that the filtration using C4Pe20 resulted in the cakes with the highest compaction, slightly closer to that of yeast cakes in the present study. Therefore, the experiments with the other model suspensions (peanut shape and polydispersed latex particles) were also run using the C4Pe20 to compare with yeast experiments. In addition, the filter geometry (size and pitch of the slits/pores) only influences the first blocking layers. Therefore, it is assumed that this effect can be neglected in determining the properties of thicker cake layers [1]. Hence, the results of the filtration of non-spherical and polydispersed particles on C4Pe20 filters and yeast cells on C2Pe5 filters can be reasonably compared.

2.2 Model suspensions

Four different suspensions were used: A cultivated yeast suspension of 50 h aged, corresponding to the stationary phase of yeast growth and three suspensions of model particles: spherical, non-spherical particles with peanut shape, and a size/shape polydispersed suspension (Figure 2). Particles and cells are suspended in a water – glycerin mixture for density matching between the continuous and solid phase.

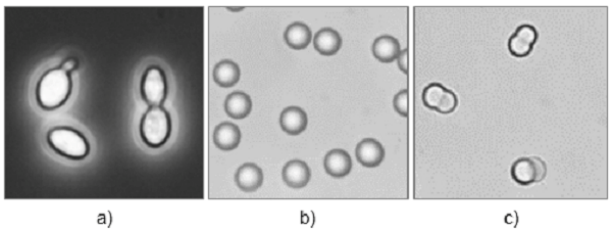

Figure 2. a) Yeast cells. b) Spherical particles. c) Non-spherical particles with peanut shape.

- The yeast suspension at a given concentration was prepared from a fresh culture harvested at the stationary state of growth (corresponding to 50 h incubated at 30 ºC and stirred at 120 rpm). The yeast *Saccharomyces cerevisiae* (Figure 2a) strain was cultivated in yeast peptone dextrose medium (YPD: 10 g/L of yeast extract, 10 g/L of dextrose and 10 g/L of bacto peptone). The correlation between the cell dry mass per unit volume and the optical density (measured at different ages of the yeast cultivation at wavelength of 600 nm) permits to relate the concentration (C_y) of cells to an easily measured parameter, the optical density (OD). The obtained correlation was C_y=0.22OD. When the cultivation reaches an age of 50 h, the sample was taken and then centrifuged. The supernatant was removed to re-suspend the cells in the density matching (1.024 g/cm^3) water – glycerin mixture (91% water, 9% glycerin). Yeast cells exhibit a size distribution ranging from 2 to 10 µm [40] when they are cultured.

- The spherical particle suspension (Figure 2b) used for the experiments consisted of latex beads (Micro Particles GmbH PS-R-8.4) of mean diameter of 8.4 µm with a standard deviation of 0.09 µm, and density of 1.055 g/cm^3 suspended in water – glycerin mixture (79%W, 21%G). Spherical particles also used in simulations, as their shape is easier to model, but also resembles the shape of individual yeast cells.

- Latex non-spherical particles (Figure 2c) with "peanut" shape (Magsphere PNT005UM) were suspended in a water – glycerin mixture (79%W, 21%G). The peanut particle longest dimension is a = 7.4 µm and is obtained by merging two spherical particles each of a diameter 5.1 µm. The particle density is 1.055 g/cm³. This particle mimics the budding yeast shape.

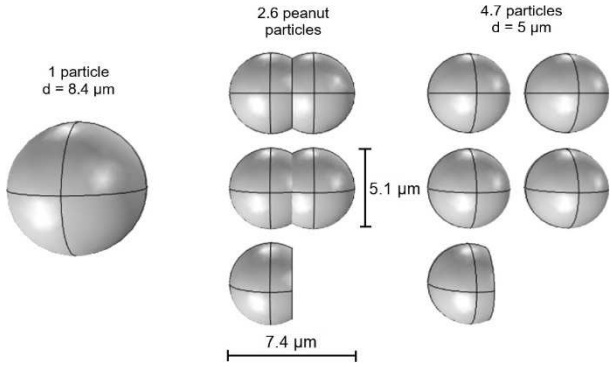

Figure 3. Poly dispersed particles suspension equally apportioned in volume with different number concentration: for 1 spherical particle of 8.4 µm diameter there are 2.6 peanut shape particles and 4.7 spherical particles with a 5µm diameter.

- The polydispersed particle suspension consisted of a discrete distribution of three types of model particles equally apportioned in volume (different number concentration as indicated in Figure 3). Two spherical particles with diameters of 5.0 and 8.4 µm (Micro Particles GmbH) and non-spherical particles with peanut shape (Magsphere PNT005UM) were suspended in the water – glycerin mixture (79%W, 21%G). This suspension was used to model the suspension of yeast cells in terms of shape (budding and individual cells) and size distribution.

Table 2 summarizes the main information of the four suspensions:

Table 2. Characteristics of the different suspensions

Code	Description	Characteristics	Specific surface, S_p x10^6 (1/m)
Yeast	Saccharomyces Cerevisiae	Cultivated 50 h aged	1.13
S	Spherical	d = 8.4 µm	1.10
NS	Non-spherical "peanut"	a = 7.4 µm; d=5.1 µm	0.71
SD	Polydisperse	$S_{8\mu m}$-NS-$S_{5\mu m}$ (1:1:1 Vol.)	0.98

2.3 Image processing

A specialized Python code is used to quantify the morphology and the transport properties of the cakes from the acquired sequence of images. The code is based on three modules, the particle velocimetry module (PVM), the particle concentration module (PCM) and the cake growth monitoring module (CGM). These three modules allow extracting the average velocity U at which particles approach the membrane, the concentration above the filtering surface C, the measured average cake height $\bar{h}_o$ and the deposited mass per membrane surface m. For more details on the code algorithm refer to the previous article [1].

2.3.1 Data analysis

The integration of the concentration $C(t)$ (% V/V) and the average velocity $U(t)$ correspond to the observed cake height $\bar{h}_o$ of matter deposited at time t, when taking into account the porosity ϵ:

$$\frac{\int UCdt}{1-\epsilon} = \bar{h}_o$$

Eq. 1

This approach is accurate since the whole channel depth remains within the optical thickness and scope of the observation set up. Hence, the information lost in depth when calculating the concentration and the cake height is negligible. The Eq. 1 allows to estimate the porosity from the information extracted using image processing.

The Darcy equation and the Carman-Kozeny formula are used to study the behavior of the Kozeny coefficient K_K throughout the filtration as a function of the pressure and the estimated porosity. The filtration velocity is assumed to be equal to the average particle velocity as there is no slip velocity in Stokes regime for density-matched particles, i.e., neutrally buoyant particles:

$$U = \frac{\Delta P}{\mu\left(R_m + \frac{\bar{h}_o K_k S_p^2 (1-\epsilon)^2}{\epsilon^3}\right)}$$

Eq. 2

with ΔP (Pa) the pressure difference, μ (Pa·s) the dynamic viscosity of the fluid, R_m (1/m) the membrane hydraulic resistance and S_p (1/m) the specific surface of the particles. The term in parentheses of Eq. 3 corresponds to the total hydraulic resistance. Here it is assumed that the commonly used resistance-in-series model can be applied as follows: $R_t = R_m + R_c$.

The different components of the total resistance $R_t = R_m + R_c$ (1/m) are calculated from the experimental data. Using the Darcy equation, the membrane hydraulic resistance $R_m = \Delta P_0/(\mu U_0)$ can be calculated from the initial operating conditions for the clean membrane. Then, as the cake forms the cake hydraulic resistance is calculated as $R_t - R_m$. Then the permeability of the cake $K_c = \bar{h}_o/R_c$ (m^2) is used as the macroscale variable to evaluate the filtration performance throughout the experiment.

In order to analyze the compressibility of the cakes formed by different particle suspensions the hydraulic resistance is expressed in terms of the deposited mass per membrane surface unit m (kg/m^2) and the cake specific resistance α_c (m/kg):

$$R_c = \alpha_c m$$

Eq. 3

Where the mass per membrane surface unit $m = CU\rho/S$ is calculated using the concentration C from the PCM, the average velocity U from the PVM, the particle/yeast cell density ρ and the membrane surface.

The compressibility has an effect on the specific resistance, which is analyzed using a power law as a function of the pressure:

$$\alpha_c = \beta \Delta P_c^n$$

Eq. 4

where β is the specific resistance coefficient and n is the compressibility index.

In the previous paper [1], the microsystem performance for the filtration of monodispersed rigid spherical particles was studied. The results obtained were validated with numerical simulations using COMSOL Multiphysics software. Indeed, the spherical shape of the particles made it possible to easily model the fluid flow in a simplified geometry that consisted of a representative unit element of the filter on which particles were regularly deposited.

3 Results and discussion

The set-up and the analysis guidelines previously described were used in all the filtration experiments of the different suspensions. The model suspension of spherical particles was used to set the experimental device and validate the analysis of the data [1]. The present paper is dedicated to the study of the filtration of yeast suspensions. To this end, the filtration of non-spherical and polydispersed solid particle suspensions was also addressed to explore two yeast features: the budding shape and the size distribution. The accumulation of cells/particles at the filter surface due to sieving was analyzed from the initial stage, when pore blocking takes place, to the transition stage when the cake progressively controls the dynamics of the filtration.

3.1 Filtration of a cultivated yeast suspension

Since the full retention of yeast cells was achieved using C2Pe5 filter units, it is thus possible to accurately assess the mass of yeast cell deposited and to perform the subsequent estimation of porosity, permeability, Kozeny coefficient and specific resistance of the cake. The results obtained for four identical experiments are presented in the form of the mean value with standard deviation to evaluate the reproducibility.

3.1.1 Cake growth

The cake average height as a function of the deposited mass per unit filter surface is plotted in Figure 4. The experiments were reproducible within a small standard deviation. A steep slope characterizes the initial blocking stage of the cake formation. The rate of cake growth is higher at the beginning of the experiment due to the heterogeneity of surface. However, this spatial heterogeneity is rapidly compensated by the consequent non-uniform permeability. Indeed, as the first particles deposited are not homogeneously distributed over the membrane surface at the beginning of the filtration, some regions of the membrane remain open to the flow, i.e., regions with higher permeability; hence the next particles are subsequently driven towards these regions to progressively cover them, thereby flattening the cake surface.

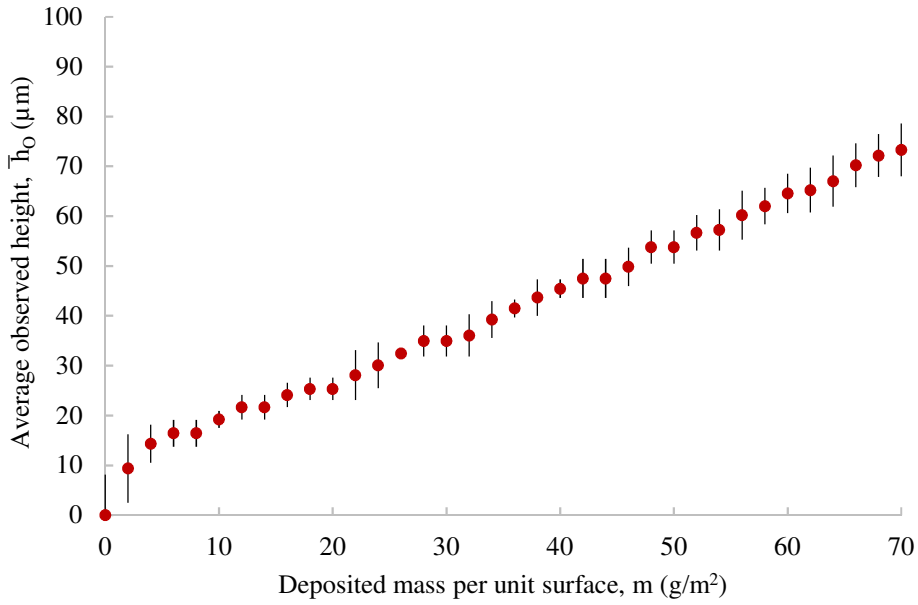

Figure 4. Yeast cakes average height as a function of the deposited mass per unit filter surface *m*.

3.1.2 Porosity permeability and Kozeny coefficient

The estimated porosity ϵ and the macroscopic properties calculated using the raw data as the cake permeability K_C, Kozeny coefficient K_K and cake specific resistance α_c were used henceforth to characterize and to compare the filtration of the different suspensions. Figure 5 shows the porosity evolution from 0.43 when the first few layers (3 – 4) layers of yeast cake are formed to 0.15 at the end of the filtration run, with pressure ranging from 0 to 13000 Pa under constant flow of 10 µl/min. Different authors report porosity values for different microorganisms ranging from 0.40 to 0.10. Fane et al. [41] found porosity values for cakes of *E. coli* cells varying from 0.18 to 0.10 for a pressure difference of ~30000 Pa. Nakanishi et al. [42] estimated the porosity for suspensions of different strains of microorganism. Particularly for yeast, they found values from 0.30 to 0.20 for pressures ranging from 13000 to 78000 Pa. For the last study, it is important to note that the estimate of the porosity was done for a much thicker cake layer (5.15 kg/m^2) than that of the present study. Ben Hassan et al. [43] used confocal laser scanning microscopy (CLSM) to characterize the deposit of fluorescent dyed yeast in dead-end filtration. Using two different microsieves units with 0.8 and 2.0 µm pore size, they found cake porosities of 0.12 and 0.10, respectively. These porosity estimates were obtained when the microsieve was fully covered (~ 30 µm thickness) and they are in fair agreement with the results of Beaufort et al. [32] who found, also using CLSM, porosities varying from 0.09 to 0.13 for yeast cakes of ~30 µm thickness using 0.2 µm membranes. All these values of porosity given by other authors are in reasonable agreement with the values of porosity obtained in the present study.

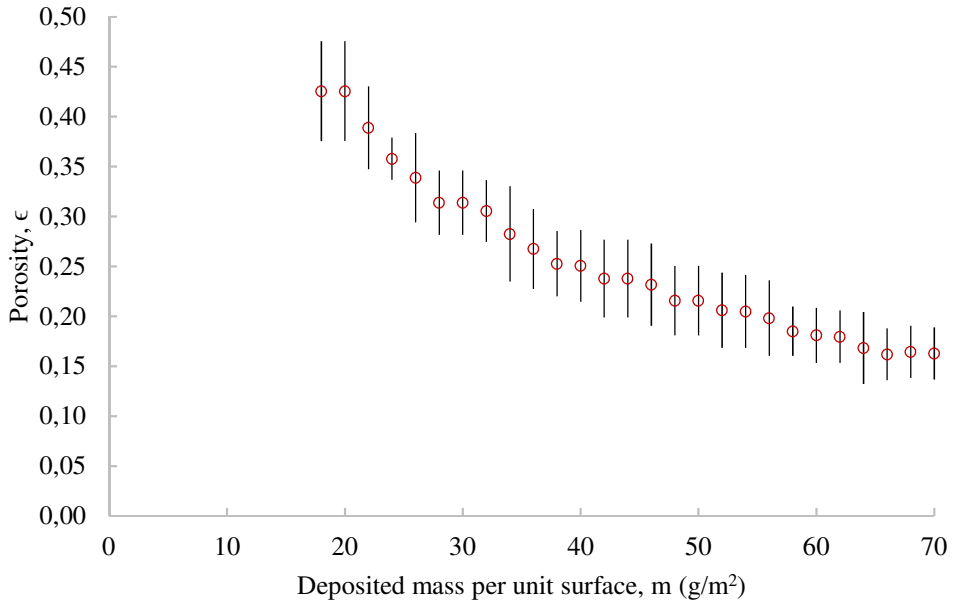

Figure 5. Porosity evolution as a function of the deposited mass per unit surface.

It can be noticed that the final porosity of yeast cakes is lower compared to the lowest porosity values calculated using theoretical packing models of spherical monodispersed and polydispersed particles. For monodispersed particles the densest regular packing for face-centered cubic and hexagonal closed-pack is equal to 0.26 [44], while for polydispersed particles the porosity value is about 0.29 [45], [46]. This significant difference between the experimental and theoretical values could be reasonably explained by the fact that the theoretical models consider only spherical particles and do not take into account the complexity addressed by living microorganisms that could exhibit a large heterogeneity in terms of shape and mechanical properties. This is the case of yeast culture in batch mode, where cells exhibit different physiological state related to their age. The influence of these characteristics on the morphology of yeast cakes is highlighted in the next sections through comparisons with two model suspensions: non-spherical monodispersed particles and a mixture of spherical and non-spherical polydispersed particles.

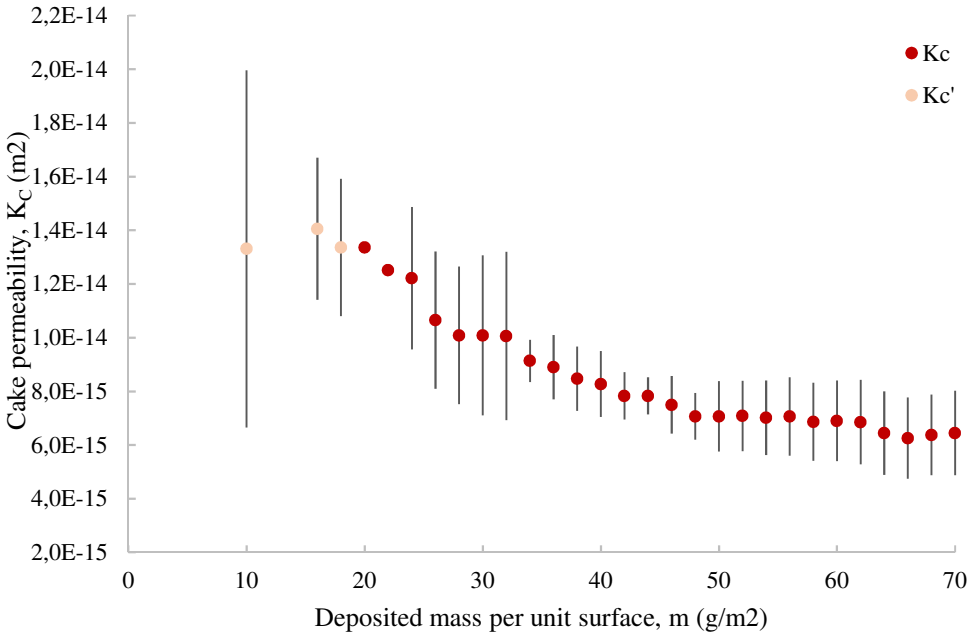

Figure 6. Evolution of the cake permeability during the filtration of the suspension of yeast cells as a function of the deposited mass per unit surface. K_C corresponds to the permeability for a formed deposit (m > 20 g/m^2) while K_C' the filter blocking layers.

Regarding the transport property of the cake in terms of the permeability, as could be expected, cake permeability decreases as a function of the mass deposited (Figure 6) in agreement with the decrease of the cake porosity. The permeability and porosity are calculated for a deposited mass higher than 20 g/m^2, this corresponds to a cake height of 24 µm and approximately to 4 layers of yeast cells (assuming a mean cell diameter of 6 µm [40]). For a deposited mass lower than 20 g/m^2, the filtration is in the pore blocking stage and the deposit is not well constituted. Accordingly, the permeability is higher at the beginning of the filtration as the cake is more porous and the resistance to fluid flow is then lower. While the filtration continues, yeast cells continue to deposit on the cake and the pressure difference across the cake rises, thus promoting a reorganization of the cake structure. Smaller or slightly deformed yeast cells can fill the spaces between the bigger cells and some of the voids inside the cake can also collapse. Thereby, the porosity decreases, and the fluid flows through smaller pathways inside the cake causing a higher hydraulic resistance and a lower permeability.

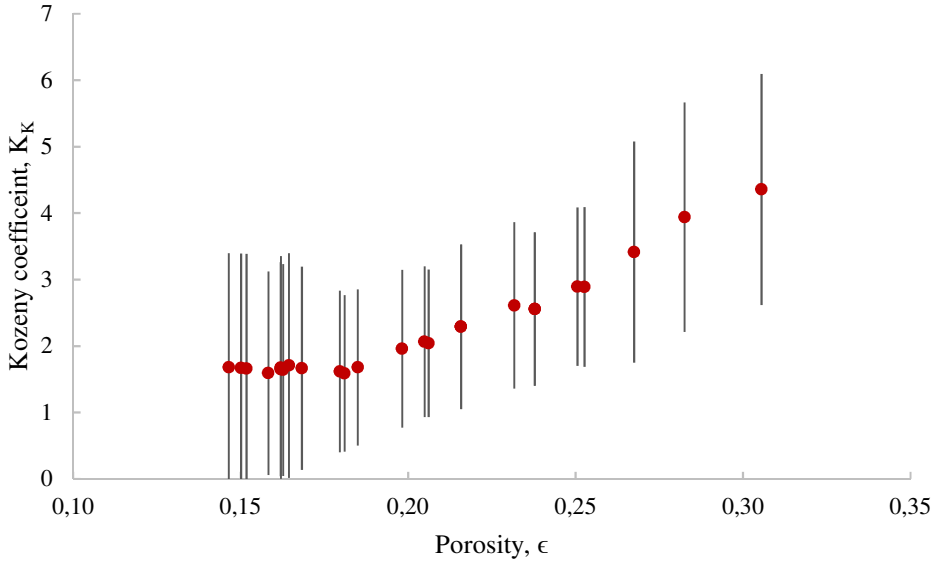

Figure 7. Kozeny coefficient as a function of the porosity for yeast cakes.

For the Carman-Kozeny formula, the non-spherical shape of the yeast cells and their size distribution (ranging from 2 to 10 µm [40] when they are cultured) influence the value of K_K, which depends on the tortuosity of the porous medium and on the pore shape. When there is an evolution of the deposit properties, K_K could differ from what is usually adopted in the literature when the Carman-Kozeny formula is used to model the permeability of a porous medium. It is then useful to estimate K_K from the cakes obtained for the filtration of yeast in the current experiments. As seen before, the porosity is related to the flow channels inside the porous medium (tortuosity and pore shape). K_K is plotted as a function of the porosity (Figure 7) to clearly illustrate this effect. The Kozeny coefficient exhibits an increasing behavior ranging from ~1.7 to 4.4; also, for porosity values lower than 0.20, it appears that K_K reaches a minimum value of ~1.7. In the work by Beaufort [32], K_K was also calculated for yeast cakes; these authors obtained K_K varying from 1 to 10 for porosity values in the range of 0.10 to 0.25. This is roughly in the same range as the present results. The exponential increasing behavior of the Kozeny coefficient could suggest that yeast cell reorganization in the cake is not the single phenomenon responsible for the variation as it was for the rigid spherical particles in the previous study [1]. Not only the polydispersity of the yeast cells but also the cell local deformation and/or compressibility should play a significant role on cake compaction. This will be shown below.

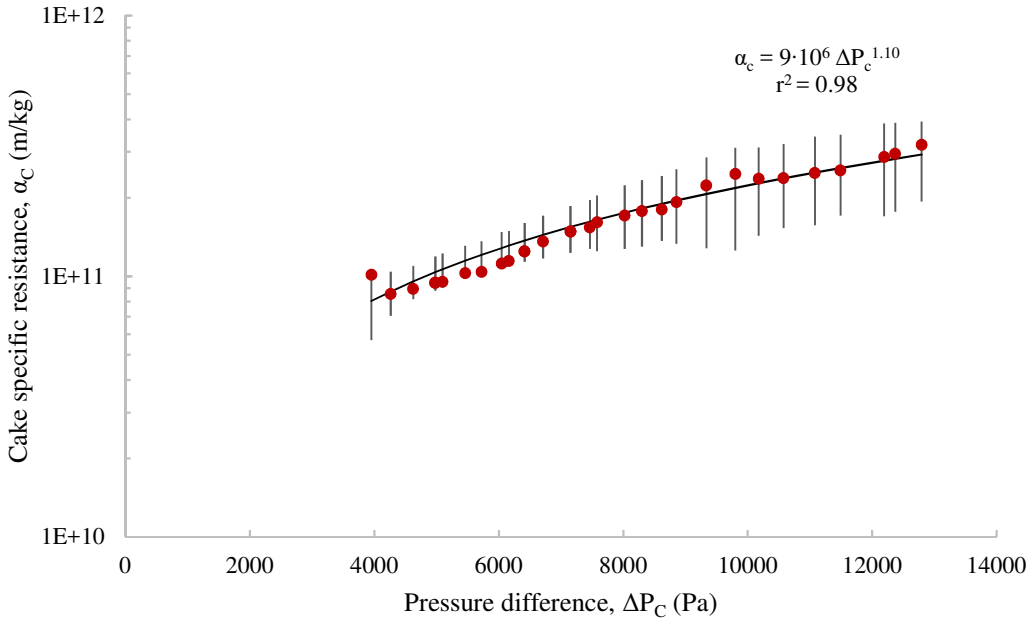

Figure 8. Yeast cake specific resistance as a function pressure drop across the cake.

An approach commonly used to study the compressibility of a cake is to analyze the specific resistance of the cake as a function of the pressure drop across the cake. As can be seen in Figure 8 the specific resistance is not constant. A power law was used to model the variations of the specific resistance with pressure drop and reflects the compressibility feature of the yeast cake. For the current experiments, a compressibility index (Eq. 4) n = 1.10 was determined by a regression analysis with a correlation r^2 = 0.98. In previous studies yeast cakes exhibited a compressible behavior with n ranging from 0.25 to 0.9 [21], [40], [47]. This rather wide variation of n could be explained by the mechanical properties of the yeast cells in the suspensions, which could change depending on the cell growth stage considered and viability. Recall that for $n > 0$ the cake is considered as compressible and highly compressible cakes have $n > 1$ [48]. The specific resistance values obtained in the current experiments were also in a consistent range compared with those previously reported in literature, where $\alpha = 10^{11} - 10^{12}$ m/kg [21], [40], [42], [47].

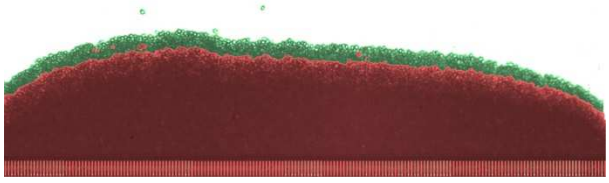

Figure 9. Yeast cake at the end of the filtration test. The red surface corresponds to the cake at the final pressure, while the green surface corresponds to the cake expansion when the final pressure is removed.

Finally, the compressibility of the cake was also observed when releasing the pressure of the system at the end of the experiment, after cake was already formed. Yeast cake relaxation was clearly confirmed by the significant volume expansion as depicted in Figure 9. The relaxed cake porosity rises to 0.26. When considering the deformation $\Delta\bar{h}_o$ of the cake average height $\bar{h}_o$ and the stress in the normal direction of the cake $\sigma = \Delta P$, related to the relaxation, it is possible to estimate an "apparent Young's modulus" of 30 KPa for the yeast cake. Previous work on the mechanical properties of yest cells [49] estimated the Young's modulus of the cell wall around ~107 MPa for individual cells at the stationary phase of growth; this value is several order of magnitude higher than the one of the cake. Also, in the work of Delarue [50], packed yeast cells exhibited wall and shape deformation when exposed to 0.5 MPa compression. More work should be addressed to better understand the nature of yeast cake compressibility and the living cells properties and behavior that explain it.

3.2 Comparison of yeast cells and model particles filtration

According to the previous results for the filtration of spherical particle suspensions [1], the following analysis for model particles (non-spherical and polydispersed particle suspensions) is performed using C4Pe20 units, for which the cakes were proved to be more compact and thus closer to yeast cake characteristics. The different variables related to the

filtration cakes for the four suspensions studied, i.e., the porosity, the permeability, the Kozeny coefficient and the specific resistance, are shown in Figure 10. First, it can be observed that cakes of spherical and non-spherical monodispersed particles exhibit similar characteristics (Figure 10). The shapes of the two model monodispersed particles could explain this matching behavior. Indeed, the peanut shape could be described as the merging of two spherical particles. This merging geometry resembles a spherocylindrical shape and particularly, spherocylindrical shapes of low aspect ratio $\alpha = a/d \in [0, 2]$ (geometric parameters a and d for peanut particles in Table 2, $\alpha = 0$ corresponds to spheres). This may lead to a similar organization in the cake and consequently a similar porosity, which is clearly observed in Figure 10b. For the current peanut particles $\alpha \sim 1.5$, the cake porosity of 0.38 at the end of the filtration run is in agreement with results of Williams and Philipse [51], for which porosities of 0.34 and 0.38 were found for $\alpha = 1$ and 2, respectively. Other authors also found similar results for spherocylindrical shapes as a function of α [52]–[54]. Accordingly, both suspensions exhibited a nearly matching cake growth for similar porosity variations (Figure 10a).

Despite the similar behavior in terms of cake growth and porosity for monodispersed suspensions (Spherical "S" and peanut shape "NS"), the shape difference has an effect on K_K. The Kozeny coefficient varies in a lower range for peanut particles than for spherical particles and was consistently lower than the common value of 5 as shown in Figure 10c. This can be explained by the difference in the specific surface (Table 2), with which K_K exhibits an inverse relation. The Kozeny coefficient appears to vary linearly with the porosity in the whole range of the experiment for the peanut particle cakes. However, for the spherical particle cakes K_K decreases linearly when the porosity varies from 0.5 to 0.4. For a porosity value lower than 0.4, K_K seems to stabilize around 7. The porosity remains higher than 0.36, which could suggest that the cake formed with spherical particles reaches a stable particle arrangement.

The similar characteristics of cakes made of monodispersed model particles suggests the importance of analyzing the filtration cakes of polydispersed particles. To this end, model suspensions with both particles of different shapes and sizes were filtered using the microfiltration units. In the current experiments, both the size and shape dispersion were chosen to be close to those of cultivated yeast cells (*Saccharomyces cerevisiae*). For 50 h aged cells, a previously reported size distribution [40] showed an important fraction of individual cells which size ranges from 4 to 8 µm. They are correctly modelled by the polydispersed model suspension. In addition, the budding cells are comparable to the non-spherical "peanut" shape. By this means, the polydisperse suspension can be considered as a simplified but realistic model of the yeast cell suspension.

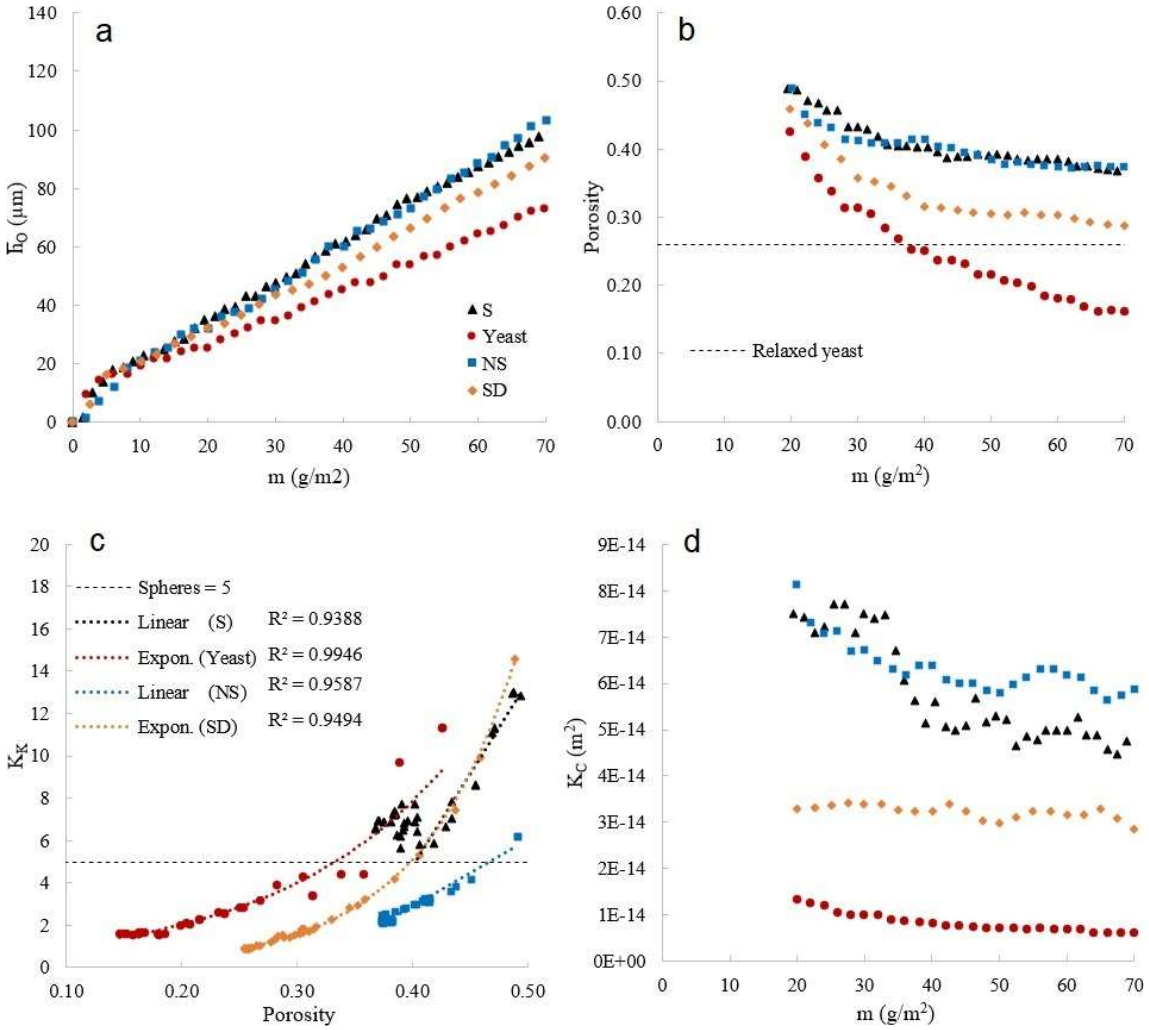

Figure 10. Comparison of the cake formed by different suspensions. a) Cake growth throughout the filtration. b) Evolution of the mean porosity of the cakes. c) Kozeny coefficient as a function of the porosity. d) Permeability of the cake

It can be seen in Figure 10a that the height of the yeast cakes is the lowest for the studied range of deposited mass, i.e., the yeast cake is the most compact for a same deposited mass. The cake height of the polydispersed particle cake is intermediate between the monodispersed particles and the yeast cells. The porosity values for the cakes obtained for the filtration of the different suspensions also confirms that the yeast cake is the most compact. It can still be noticed that the porosity and permeability analysis starts at 20 g/m^2, after the first membrane blocking phase (2 – 3 layers for monodispersed particles and 3 – 4 for yeast and the polydispersed particles) is finished as previously explained. It is remarkable that the porosity curves start from different values for the different suspensions and this difference becomes larger as the cakes continue forming during the filtration (Table 3); this highlights the role of more complex mechanisms involved in cake compaction.

Table 3. Summary of the porosity evolution for the four suspensions.

Suspension	Initial porosity ϵ_0 (at 20 g/m^2)	Porosity reduction (at 70g/m^2)
S	0.49	25%
Yeast	0.43	62%
NS	0.49	25%
SD	0.46	37%

Table 3 shows a consistent reduction of the porosity for the different suspensions. In the case of monodispersed particles the porosity decreasing is related with the initial influence of membrane structure on the first particle layer and the transition to a more random arrangement as it is explained with more detail in a previous article [1]. A similar phenomenon occurs for polydispersed model particles, the initial influence of the membrane geometry decreases rapidly to a random

arrangement. These results illustrate more clearly the role of polydispersity on the filtration performance. The polydispersity of the suspension is associated with a lower cake porosity. Indeed, the smaller particles can fill the voids around the bigger particles, which reduces the void fraction of the cake. This phenomenon has been previously observed experimentally and modeled theoretically. Ben Hassan [33] observed this phenomenon and this particle arrangement for a bi-dispersed suspension (4.8 and 1 µm latex beads). A porosity of 0.40 was found for the bi-dispersed particle cake, whereas for monodispersed particles the porosity was 0.45 and 0.42, for 4.8 and 1 µm particles, respectively. Similar results in term of particle arrangement have also been described by Thies-Weesie and Philipse [55]. Other authors concluded that particle packing depends on the particle size ratio and the mixing percentage of the particles of different sizes [45], [46], [55], [56]. The permeability evolution in the current experiment is also consistent with the previous analysis of the porosity (Figure 10d) as a lower permeability was found for yeast and polydispersed particle cakes. In the current study we cannot quantitatively assess the effect of pressure on particle/cells rearrangement in the cake, however the raising pressure can be another parameter triggering this rearrangement that contributes to porosity reduction.

The Kozeny coefficient increases exponentially with the porosity for yeast and polydispersed particles cakes in contrast with the linear increase exhibited by monodispersed particles. Ozgumus et al. [57] found previously this linear relationship simulating the flow through a porous media formed by rod-like particles (similar to peanuts in shape). K_K values within the range of about 3 to 12 were reported for porosities between 0.2 to 0.4. The different tendency could be explained by the different re-organization mechanism in the cake when there is a particle size distribution.

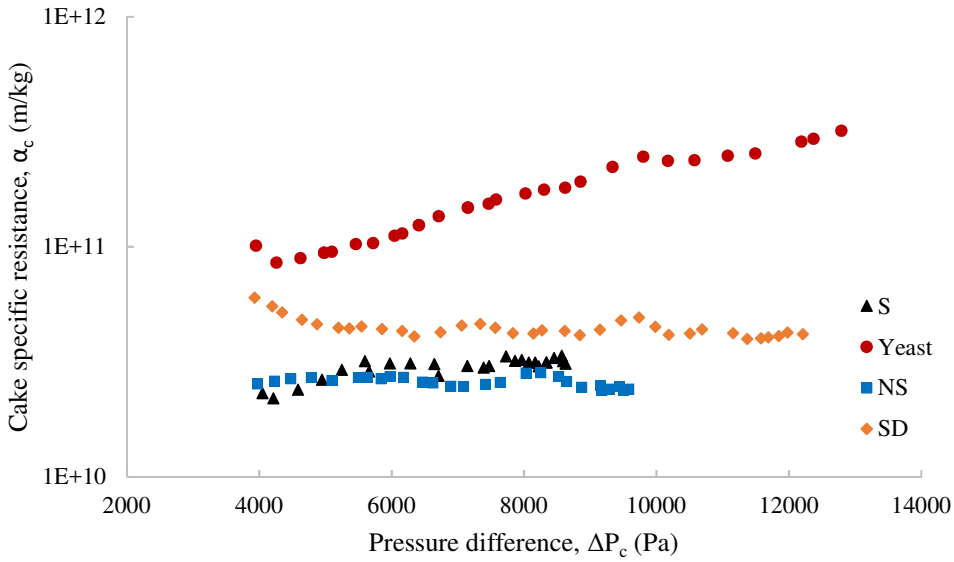

Figure 11. Comparison of the cake specific resistance as a function of the pressure drop across the cake

However, even though the suspension polydispersity can partly explain the high compaction of the yeast cake; there remains a significant gap between the results obtained for the cake of yeast cells and polydispersed particles, as highlighted in Figure 10. This is also confirmed in Figure 11, which depicts the variations of the specific resistance of the cake as a function of the pressure drop across the cake. On one hand, all the cakes formed by solid particles exhibit an incompressible behavior as the compressibility index $n = 0$. This means that the specific resistance scatters around the mean value and so it is constant and independent of the pressure. On the other hand, a compressibility index $n = 1.1$ was found for the yeast cake, which corresponds to a highly compressible behavior and is in reasonable agreement with what has been reported in the literature. In addition, only yeast cake exhibited a volume expansion after releasing the pressure at the end of the experiment, as shown in Figure 9. The analysis of this expansion indicates a porosity increase after relaxation from $\epsilon \sim 0.15$ to 0.26 (Figure 10b). It is interesting that this final value is close to the one estimated for the polydispersed particle suspension at the end of the filtration run ($\epsilon \sim 0.29$). This supports the behavior depicted by the specific resistance and confirms that the lower permeability of the yeast cake can be explained by the combined effect of the polydispersity of the cells and the compressibility of the cake possibly owing in part to slight deformability leading to reversible compaction.

4 Conclusion

The experimental protocol described here is a suitable approach to study the formation and the properties of the filtration cakes obtained for various suspensions. The experimental set-up and the analysis protocol were validated for the filtration of monodispersed spherical particles suspensions in a previous article [1]. In order to investigate the effect of multi-scale characteristics of complex suspensions, filtration of cultivated yeast (*Saccharomyces cerevisiae*) suspensions were performed. The cakes of monodispersed non-deformable particles exhibited a similar incompressible behavior with relatively high permeability. This result is in good agreement with the cake porosity, which varied in the range 0.50 – 0.36. This corresponds to characteristic packing models from loosest regular packing to random close packing, respectively. The different particle shapes examined in the current experiment did not change the overall hydrodynamics of the filtration, this could be explained by the relative similar shape of spherical an peanut shape particles, which can be assimilated to two merged spheres; only the Kozeny coefficient was affected, as it is strongly dependent on the porous medium geometry related to the particle geometry.

The polydispersity of the particles proved to be one of the major features playing a role on the filtration properties of yeast cakes. However, it was not responsible for the compressibility of the yeast cake with the pressure increase. Yeast cake exhibited the lowest porosity around 0.15 and the cake of polydispersed particles exhibited and intermediate porosity of 0.29 between monodispersed and yeast cakes. This intermediate behavior was also observed for the cake permeability. The low permeability of the yeast cakes was due to the combined effect of the polydispersity of the yeast cells and the compressibility of the cake. In addition, after pressure relaxation ($\Delta P = 0$), only the yeast cake expanded. This supports the hypothesis of yeast cake compressibility. The estimated yeast cake porosity after relaxation is around 0.26, which is closer to the one of the polydispersed particles.

It remains to explain the nature of this compressibility as previous studies reported low yeast cell deformation for the range of pressures in these experiments. Indeed, this low deformability corresponds to higher Young's modulus than the value of 30 kPa estimated based on the yeast cake relaxation experiment. Further experiments could investigate the effect of yeast cell mechanical properties by filtering yeast at different ages and physiological states.

Acknowledgments

This work was done in the frame of the research grant program AAP 2015 from Idex UNITI "NEMESIS" conv-ANR-11Idex-0002-02.

The authors thank Pierre Joseph from the « Laboratoire d'analyse et d'architecture des systèmes » (LAAS).

References

[1] A. Valencia, C. Le Men, C. Ellero, C. Lafforgue-Baldas, P. Schmitz, and J. F. Morris, "Direct observation at the microscale of particle deposition during the first stage of the microfiltration process," *J. Membr. Sci.*, vol. 599, p. 117823, Apr. 2020, doi: 10.1016/j.memsci.2020.117823.

[2] C. Charcosset, "Procédés membranaires à application pharmaceutique et biotechnologique," *ITBM-RBM*, vol. 27, no. 1, pp. 1–7, Feb. 2006, doi: 10.1016/j.rbmret.2005.10.003.

[3] L. Qin *et al.*, "Anoxic oscillating MBR for photosynthetic bacteria harvesting and high salinity wastewater treatment," *Bioresour. Technol.*, vol. 224, pp. 69–77, Jan. 2017, doi: 10.1016/j.biortech.2016.10.067.

[4] W. Pronk *et al.*, "Gravity-driven membrane filtration for water and wastewater treatment: A review," *Water Res.*, vol. 149, pp. 553–565, Feb. 2019, doi: 10.1016/j.watres.2018.11.062.

[5] A. Bennett, "Innovation trends in food and beverage filtration applications," *Filtr. Sep.*, vol. 52, no. 2, pp. 28–33, Mar. 2015, doi: 10.1016/S0015-1882(15)30091-4.

[6] E. Dressaire and A. Sauret, "Clogging of microfluidic systems," *Soft Matter*, vol. 13, no. 1, pp. 37–48, Dec. 2016, doi: 10.1039/C6SM01879C.

[7] S. Xue, C. Li, J. Li, H. Zhu, and Y. Guo, "A catechol-based biomimetic strategy combined with surface mineralization to enhance hydrophilicity and anti-fouling property of PTFE flat membrane," *J. Membr. Sci.*, vol. 524, pp. 409–418, Feb. 2017, doi: 10.1016/j.memsci.2016.11.075.

[8] A. Kowalik-Klimczak, E. Woskowicz, and J. Kacprzyńska-Gołacka, "The surface modification of polyamide membranes using graphene oxide," *Colloids Surf. Physicochem. Eng. Asp.*, vol. 587, p. 124281, Feb. 2020, doi: 10.1016/j.colsurfa.2019.124281.

[9] J. Liu, Z. Liu, X. Xu, and F. Liu, "Saw-tooth spacer for membrane filtration: Hydrodynamic investigation by PIV and filtration experiment validation," *Chem. Eng. Process. Process Intensif.*, vol. 91, pp. 23–34, May 2015, doi: 10.1016/j.cep.2015.03.013.

[10] Y. Z. Tan *et al.*, "Enhancing fouling mitigation of submerged flat-sheet membranes by vibrating 3D-spacers," *Sep. Purif. Technol.*, vol. 215, pp. 70–80, May 2019, doi: 10.1016/j.seppur.2018.12.085.

[11] Y. P. Zhang, A. W. K. Law, and A. G. Fane, "Determination of critical flux by mass balance technique combined with direct observation image analysis," *J. Membr. Sci.*, vol. 365, no. 1, pp. 106–113, Dec. 2010, doi: 10.1016/j.memsci.2010.08.047.

[12] E. Iritani, N. Katagiri, and G. Inagaki, “Compression and expansion properties of filter cake accompanied with step change in applied pressure in membrane filtration,” *Sep. Purif. Technol.*, Apr. 2017, doi: 10.1016/j.seppur.2016.11.067.
[13] J. Mendret, C. Guiguir, C. Cabassud, and P. Schmitz, “Dead-end ultrafiltration and backwash: dynamic characterisation of cake properties at local scale,” *Desalination*, vol. 199, no. 1, pp. 216–218, Nov. 2006, doi: 10.1016/j.desal.2006.03.164.
[14] W. D. Mores and R. H. Davis, “Direct visual observation of yeast deposition and removal during microfiltration,” *J. Membr. Sci.*, vol. 189, no. 2, pp. 217–230, Aug. 2001, doi: 10.1016/S0376-7388(01)00409-4.
[15] P. Schmitz, B. Wandelt, D. Houi, and M. Hildenbrand, “Particle aggregation at the membrane surface in crossflow microfiltration,” *J. Membr. Sci.*, vol. 84, no. 1, pp. 171–183, Sep. 1993, doi: 10.1016/0376-7388(93)85059-6.
[16] T. van de Laar, S. ten Klooster, K. Schroën, and J. Sprakel, “Transition-state theory predicts clogging at the microscale,” *Sci. Rep.*, vol. 6, p. 28450, Jun. 2016, doi: 10.1038/srep28450.
[17] B. Mahamadou Harouna, O. Benkortbi, S. Hanini, and A. Amrane, “Modeling of transitional pore blockage to cake filtration and modified fouling index – Dynamical surface phenomena in membrane filtration,” *Chem. Eng. Sci.*, vol. 193, pp. 298–311, Jan. 2019, doi: 10.1016/j.ces.2018.07.054.
[18] C.-C. Ho and A. L. Zydney, “A Combined Pore Blockage and Cake Filtration Model for Protein Fouling during Microfiltration,” *J. Colloid Interface Sci.*, vol. 232, no. 2, pp. 389–399, Dec. 2000, doi: 10.1006/jcis.2000.7231.
[19] L. Hou, Z. Wang, and P. Song, “A precise combined complete blocking and cake filtration model for describing the flux variation in membrane filtration process with BSA solution,” *J. Membr. Sci.*, vol. 542, pp. 186–194, Nov. 2017, doi: 10.1016/j.memsci.2017.08.013.
[20] M. Meireles, M. Clifton, and P. Aimar, “Filtration of yeast suspensions: experimental observations and modelling of dead-end filtration with a compressible cake,” *Desalination*, vol. 147, no. 1, pp. 19–23, Sep. 2002, doi: 10.1016/S0011-9164(02)00565-9.
[21] M. Meireles, C. Molle, M. J. Clifton, and P. Aimar, “The origin of high hydraulic resistance for filter cakes of deformable particles: cell-bed deformation or surface-layer effect?,” *Chem. Eng. Sci.*, vol. 59, no. 24, pp. 5819–5829, Dec. 2004, doi: 10.1016/j.ces.2004.06.040.
[22] X. Li, J. Li, Z. Cui, and Y. Yao, “Modeling of filtration characteristics during submerged hollow fiber membrane microfiltration of yeast suspension under aeration condition,” *J. Membr. Sci.*, vol. 510, pp. 455–465, Jul. 2016, doi: 10.1016/j.memsci.2016.03.003.
[23] V. Chen, H. Li, and A. G. Fane, “Non-invasive observation of synthetic membrane processes – a review of methods,” *J. Membr. Sci.*, vol. 241, no. 1, pp. 23–44, Sep. 2004, doi: 10.1016/j.memsci.2004.04.029.
[24] T. Schluep and F. Widmer, “Initial transient effects during cross flow microfiltration of yeast suspensions,” *J. Membr. Sci.*, vol. 115, no. 2, pp. 133–145, Jul. 1996, doi: 10.1016/0376-7388(95)00321-5.
[25] V. L. Vilker, C. K. Colton, and K. A. Smith, “Concentration polarization in protein ultrafiltration. Part II: Theoretical and experimental study of albumin ultrafiltered in an unstirred cell,” *AIChE J.*, vol. 27, no. 4, pp. 637–645, Jul. 1981, doi: 10.1002/aic.690270416.
[26] C. R. Ethier and Daniel. C. Lin, “Refractometric measurement of polarized layer structure: studies of hyaluronic acid ultrafiltration,” *J. Membr. Sci.*, vol. 68, no. 3, pp. 249–261, Apr. 1992, doi: 10.1016/0376-7388(92)85026-F.
[27] P. Le-Clech, Y. Marselina, Y. Ye, R. M. Stuetz, and V. Chen, “Visualisation of polysaccharide fouling on microporous membrane using different characterisation techniques,” *J. Membr. Sci.*, vol. 290, no. 1–2, pp. 36–45, Mar. 2007, doi: 10.1016/j.memsci.2006.12.012.
[28] V. Chen, H. Li, and A. G. Fane, “Non-invasive observation of synthetic membrane processes – a review of methods,” *J. Membr. Sci.*, vol. 241, no. 1, pp. 23–44, Sep. 2004, doi: 10.1016/j.memsci.2004.04.029.
[29] J. Mendret, “Mise au point de méthodes de caractérisation non destructives du colmatage de membranes : application à la caractérisation in situ d’un dépôt particulaire en ultrafiltration frontale en lien avec les performances du procédé,” thesis, Toulouse, INSA, 2007. Accessed: Oct. 21, 2019. [Online]. Available: http://www.theses.fr/2007ISAT0050
[30] S. Lorenzen, Y. Ye, V. Chen, and M. L. Christensen, “Direct observation of fouling phenomena during cross-flow filtration: Influence of particle surface charge,” *J. Membr. Sci.*, vol. 510, pp. 546–558, Jul. 2016, doi: 10.1016/j.memsci.2016.01.046.
[31] N. Delouche, J. M. van Doorn, T. E. Kodger, A. B. Schofield, J. Sprakel, and H. Tabuteau, “The contribution of colloidal aggregates to the clogging dynamics at the pore scale,” *J. Membr. Sci.*, vol. 635, p. 119509, Oct. 2021, doi: 10.1016/j.memsci.2021.119509.
[32] S. Beaufort, “Développement d’outils et de méthodologies pour l’étude de l’organisation et de la localisation in vivo de micro-organismes dans des structures biologiques complexes,” thesis, Toulouse, INSA, 2010. Accessed: Sep. 25, 2019. [Online]. Available: http://www.theses.fr/2010ISAT0037
[33] I. B. Hassan, “Analyse multi-échelle de la filtration sur microsive de particules modèles inertes et biologiques : caractérisation in situ du dépôt par microscopie confocale,” phdthesis, INSA de Toulouse, 2014. Accessed: Jan. 10, 2018. [Online]. Available: https://tel.archives-ouvertes.fr/tel-01073549/document
[34] I. Ben Hassan, C. Lafforgue, A. Ayadi, and P. Schmitz, “In situ 3D characterization of monodispersed spherical particle deposition on microsieve using confocal laser scanning microscopy,” *J. Membr. Sci.*, vol. 454, pp. 283–297, Mar. 2014, doi: 10.1016/j.memsci.2013.12.003.

[35] I. Ben Hassan, C. Lafforgue, C. Ellero, A. Ayadi, and P. Schmitz, “Coupling of local visualization and numerical approach for particle microfiltration optimization,” *Microsyst. Technol.*, vol. 21, no. 3, pp. 509–517, Mar. 2015, doi: 10.1007/s00542-013-1906-9.
[36] P. H. Hodgson, V. I. Pillay, and A. G. Fane, “Visual study of crossflow microfiltration with inorganic membranes: resistance of biomass and particulate cake.” 1993.
[37] H. Li, A. G. Fane, H. G. L. Coster, and S. Vigneswaran, “Direct observation of particle deposition on the membrane surface during crossflow microfiltration,” *J. Membr. Sci.*, vol. 149, no. 1, pp. 83–97, Oct. 1998, doi: 10.1016/S0376-7388(98)00181-1.
[38] R. van Zwieten, T. van de Laar, J. Sprakel, and K. Schroën, “From cooperative to uncorrelated clogging in cross-flow microfluidic membranes,” *Sci. Rep.*, vol. 8, no. 1, p. 5687, Dec. 2018, doi: 10.1038/s41598-018-24088-6.
[39] P. Schmitz, D. Houi, and B. Wandelt, “Hydrodynamic aspects of crossflow microfiltration. Analysis of particle deposition at the membrane surface,” *J. Membr. Sci.*, vol. 71, no. 1, pp. 29–40, Jul. 1992, doi: 10.1016/0376-7388(92)85003-2.
[40] A. Rushton and H. E. Khoo, “The filtration characteristics of yeast,” *J. Appl. Chem. Biotechnol.*, vol. 27, no. 1, pp. 99–109, 1977, doi: 10.1002/jctb.5020270115.
[41] A. G. Fane, C. J. D. Fell, P. H. Hodgson, G. Leslie, and K. Marshall, “Microfiltration of biomass and biofluids: Effects of membrane morphology and operating conditions,” *Filtr. Sep.*, vol. 28, no. 5, pp. 332–331, Sep. 1991, doi: 10.1016/0015-1882(91)80157-Z.
[42] K. Nakanishi, T. Tadokoro, and R. Matsuno, “On the Specific Resistance of Cakes of Microorganisms,” *Chem. Eng. Commun.*, vol. 62, no. 1–6, pp. 187–201, Dec. 1987, doi: 10.1080/00986448708912059.
[43] I. Ben Hassan, C. Lafforgue, A. Ayadi, and P. Schmitz, “Study of the separation of yeast by microsieves: In situ 3D characterization of the cake using confocal laser scanning microscopy,” *Food Bioprod. Process.*, vol. 92, no. C2, pp. 178–191, 2014, doi: 10.1016/j.fbp.2013.12.012.
[44] F. A. L. Dullien, *Porous Media: Fluid Transport and Pore Structure*. Academic Press, 2012.
[45] K. W. Desmond and E. R. Weeks, “Influence of Particle Size Distribution on Random Close Packing,” *Phys. Rev. E*, vol. 90, no. 2, p. 022204, Aug. 2014, doi: 10.1103/physreve.90.022204.
[46] M. Taiebat, P. Mutabaruka, R. Pellenq, and F. Radjai, “Effect of particle size distribution on 3D packings of spherical particles,” *EPJ Web Conf.*, vol. 140, p. 02030, 2017, doi: 10.1051/epjconf/201714002030.
[47] M. Mota, J. A. C. Teixeira, and A. Yelshin, “Dependence of Saccharomyces cerevisiae filtration through membrance on yeast concentration,” 2004.
[48] A. Gupta and D. Yan, Eds., “Chapter 15 - Solid Liquid Separation – Filtration,” in *Mineral Processing Design and Operations (Second Edition)*, Amsterdam: Elsevier, 2016, pp. 507–561. doi: 10.1016/B978-0-444-63589-1.00015-0.
[49] A. E. Smith, Z. Zhang, C. R. Thomas, K. E. Moxham, and A. P. J. Middelberg, “The mechanical properties of Saccharomyces cerevisiae,” *Proc. Natl. Acad. Sci. U. S. A.*, vol. 97, no. 18, pp. 9871–9874, Aug. 2000.
[50] M. Delarue *et al.*, “Self-Driven Jamming in Growing Microbial Populations,” *Nat. Phys.*, vol. 12, no. 8, pp. 762–766, Aug. 2016, doi: 10.1038/nphys3741.
[51] S. R. Williams and A. P. Philipse, “Random packings of spheres and spherocylinders simulated by mechanical contraction,” *Phys. Rev. E*, vol. 67, no. 5, p. 051301, May 2003, doi: 10.1103/PhysRevE.67.051301.
[52] A. V. Kyrylyuk, M. A. van de Haar, L. Rossi, A. Wouterse, and A. P. Philipse, “Isochoric ideality in jammed random packings of non-spherical granular matter,” *Soft Matter*, vol. 7, no. 5, pp. 1671–1674, Feb. 2011, doi: 10.1039/C0SM00754D.
[53] A. Wouterse, S. Luding, and A. P. Philipse, “On contact numbers in random rod packings,” *Granul. Matter*, vol. 11, no. 3, pp. 169–177, May 2009, doi: 10.1007/s10035-009-0126-6.
[54] L. Meng, P. Lu, S. Li, J. Zhao, and T. Li, “Shape and size effects on the packing density of binary spherocylinders,” *Powder Technol.*, vol. 228, pp. 284–294, Sep. 2012, doi: 10.1016/j.powtec.2012.05.033.
[55] D. M. E. Thies-Weesie and A. P. Philipse, “Liquid Permeation of Bidisperse Colloidal Hard-Sphere Packings and the Kozeny-Carman Scaling Relation,” *J. Colloid Interface Sci.*, vol. 162, no. 2, pp. 470–480, Feb. 1994, doi: 10.1006/jcis.1994.1062.
[56] H. Y. Sohn and C. Moreland, “The effect of particle size distribution on packing density,” *Can. J. Chem. Eng.*, vol. 46, no. 3, pp. 162–167, 1968, doi: 10.1002/cjce.5450460305.
[57] T. Ozgumus, M. Mobedi, and U. Ozkol, “Determination of Kozeny Constant Based on Porosity and Pore to Throat Size Ratio in Porous Medium with Rectangular Rods,” *Eng. Appl. Comput. Fluid Mech.*, vol. 8, no. 2, pp. 308–318, Jan. 2014, doi: 10.1080/19942060.2014.11015516.
[58] M. Schiavone *et al.*, “Evidence for a Role for the Plasma Membrane in the Nanomechanical Properties of the Cell Wall as Revealed by an Atomic Force Microscopy Study of the Response of Saccharomyces cerevisiae to Ethanol Stress,” *Appl. Environ. Microbiol.*, vol. 82, no. 15, pp. 4789–4801, Jul. 2016, doi: 10.1128/AEM.01213-16.